On the Characterization of Novel Step-Index Biocompatible and Biodegradable poly(D,L-lactic acid) Based Optical Fiber

Agnieszka Gierej, Adam Filipkowski, Dariusz Pysz, Ryszard Buczyński, Maxime Vagenende, Peter Dubruel, Hugo Thienpont, *Member, IEEE*, Thomas Geernaert, and Francis Berghmans, *Senior Member, IEEE*

***Abstract*—We report on the first step-index biodegradable polymer optical fiber (bioPOF) fabricated using commercially available polyesters, with a core made from poly(D,L-lactic-co-glycolic acid) and a cladding made from poly(D,L-lactic acid). We prepared the preforms with a rod-in-tube technique and the fibers with a standard heat drawing process. We discuss the chemical and optical properties of the polyesters along the fabrication process from polymer granulates to optical fiber. More specifically, we address the influence of the processing steps on the molecular weight and thermal properties of the polymers. Cutback measurements return an attenuation of 0.26 dB/cm at 950 nm for fibers with an outer diameter of 1000 $\pm$ 50 μm, a core of 570 $\pm$ 30 μm, and a numerical aperture of 0.163. When immersed in phosphate-buffered saline (PBS), bioPOFs degrade over a period of 3 months, concurrent with a 91% molecular weight loss. The core decomposes already after three weeks and features 85% molecular weight loss. There is no any additional optical loss caused by immersion in PBS during the first 30–40 min for a bioPOFs with a diameter of about 500 μm. Our result demonstrates that bioPOF can be suitable for applications requiring light delivery, deep into living tissue, such as photodynamic therapy.**

***Index Terms*—Biodegradable materials, optical fibers, optical fiber materials, optical polymers, plastic optical fiber.**

Manuscript received September 18, 2019; revised November 27, 2019; accepted December 11, 2019. Date of publication December 16, 2019; date of current version April 1, 2020. This work was supported in part by Research Foundation Flanders (FWO) under Project G048915N 'Biodegradable Fiber Optic Technology for Biophotonic Applications' and Grant G0F6218N (EOS-convention 30467715). Institute of Electronic Materials Technology was supported by the Project POIR.04.04.00-1C74/16 operated within the Foundation for Polish Science Team Programme co-financed by the European Regional Development Fund under Smart Growth Operational Programme (SG OP), Priority Axis IV. *(Corresponding author: Agnieszka Gierej.)*

A. Gierej, H. Thienpont, T. Geernaert, and F. Berghmans are with the Department of Applied Physics and Photonics, Brussels Photonics (B-PHOT), Vrije Universiteit Brussel, B-1050 Brussels, Belgium (e-mail: agnieszka.gierej@vub.be; hthienpo@vub.ac.be; thomas.geernaert@vub.be; francis.berghmans@vub.be).

A. Filipkowski and D. Pysz are with the Institute of Electronic Materials Technology (ITME), 01-919 Warszawa, Poland (e-mail: adam.filipkowski@itme.edu.pl; dariusz.pysz@itme.edu.pl).

R. Buczyński is with the Institute of Electronic Materials Technology (ITME), 01-919 Warszawa, Poland, and also with the Faculty of Physics, University of Warsaw (UW), 02-093 Warsaw, Poland (e-mail: rbuczyns@igf.fuw.edu.pl).

M. Vagenende is with the Department of Applied Physics and Photonics, Brussels Photonics (B-PHOT), Vrije Universiteit Brussel, B-1050 Brussels, Belgium, and also with the Department of Organic and Macromolecular Chemistry, Polymer Chemistry and Biomaterials Group (PBM), Centre of Macromolecular Chemistry (CMaC), Universiteit Gent, B-9000 Ghent, Belgium (e-mail: maxime.vagenende@ugent.be).

P. Dubruel is with the Department of Organic and Macromolecular Chemistry, Polymer Chemistry and Biomaterials Group (PBM), Centre of Macromolecular Chemistry (CMaC), Universiteit Gent, B-9000 Ghent, Belgium (e-mail: peter.dubruel@ugent.be).

Color versions of one or more of the figures in this article are available online at http://ieeexplore.ieee.org.

Digital Object Identifier 10.1109/JLT.2019.2959945

I. Introduction

BIOCOMPATIBLE optical fibers can assist the delivery of light deep into the human body and hence they allow overcoming the typical limits of light penetration in living tissue [1]. The prospect is that these small-sized photonic devices can stay inside the body in a minimally invasive manner for a prolonged period of time and serve, for example, point-of-care medical diagnosis, continuous health monitoring or light-based therapy. If, in addition, these optical waveguides are made from biodegradable materials, they can be left inside the body after usage since they will resorb and disappear over time, which would for example avoid possible complications due to surgical removal of the device [2].

Open literature already reports on biodegradable optical fibers made from a plethora of different materials for potential applications in the biomedical field. Examples include inorganic materials such as silica [3] and calcium-phosphate glass [4], [5]; bio-derived natural materials such as cellulose [6], silk [7], [8] and hydrogels [9]–[12]; synthetic polymers such as PLLA [13], [14] and elastomers such as POC-POMC [15], as well as hybrid materials [16]. Recent and detailed reviews on this subject are published in [17]–[19].

In previous work, we have already investigated the use of amorphous polyesters to fabricate biocompatible and biodegradable polymer optical fiber (bioPOF). More specifically we have reported on unclad bioPOF made from poly(D,L-lactic acid), abbreviated as PDLLA [20]. This material shares interesting properties with other biodegradable synthetic polymers such as PLLA (poly(L-lactic acid)) and PDLGA (poly(D,L-lactic-co-glycolic acid)), i.e., relatively easy processing, good optical transparency, thermomechanical stability and controllable degradation time. Our PDLLA unclad bioPOF featured an attenuation of 0.11 dB/cm at 772 nm in air, which was the lowest loss reported thus far for polymer biocompatible waveguides [6], [10], [13]–[15]. Furthermore, we evidenced that the PDLLA fiber truly degrades, and we found that fibers with a larger diameter of 600 μm degrade faster in phosphate-buffered saline

(PBS) than those with smaller diameters of 300 and 200 μm. PDLLA fiber featured more than 84% molecular weight loss over a period of 3 months when immersed in PBS.

In this paper we investigate another commercially available biocompatible polyester that features similar thermo-mechanical properties as PDLLA, whilst offering a suitable difference in refractive index to form a core-cladding structure. We focused on poly(D,L-lactic-co-glycolic acid) or PDLGA, which is known for drug delivery [21] and tissue engineering applications [22], as well as for the fabrication of bioresorbable planar waveguides [13]. PDLGA is actually one of the most extensively studied biomaterials for biomedical applications since it allows optimizing its properties such as biodegradation rate by varying the PLA and PGA fractions. PLGA-based biocopolymers have been already commercially developed and are being applied as locally implanted medical devices [23]. An injectable and bioresorbable photonics device that consisted of a PLGA substrate and short alginate coated PLGA biofiber has recently been fabricated and was used for the continuous monitoring of cerebral temperature, oxygenation and neural activity in tissues and biofluids of mice [24]. Note that both PDLLA and PDLGA are regulated by the U.S. FDA and approved for clinical use [25].

We report on the successful fabrication of step-index bioPOF, and we pay attention to the optical characterization and degradation of these fibers in a simulated biological environment in view of assessing the actual application potential of such bioPOFs.

We organized our manuscript as follows. Section II describes the characterization of bulk PDLLA and PDLGA. Section III describes the preform preparation and heat drawing of the preforms into optical fibers. Subsequently, in section IV, we report on the T_g values, as well as on the molecular mass loss of the granulate, preforms and produced fibers in order to interpret how the thermo-mechanical and physico-chemical properties were influenced by the fabrication steps. In section V, we characterize our bioPOF from an optical standpoint. Section VI focuses on the *in vitro* degradation of the bioPOFs and reports on the immersion induced loss of the fibers in phosphate buffered saline (PBS). Section VII includes a summary and conclusion, supplemented with perspectives for future research.

II. Chemical and Optical Characterization of Bulk Polyesters

Our starting materials are PDLLA granulates (PURASORB PDL 20) with an inherent viscosity of 2.0 dl/g and PDLGA granulates (PURASORB PDLG 5010) with an inherent viscosity of 1.03 dl/g. For the latter, the comonomer ratio D,L-lactide to glycolide is 52 to 48 mol%. Both materials were purchased from Corbion Purac Biomaterials [26], [27]. The PURASORB products are registered under FDA number DMF-21817 [25].

We first characterized the granulate materials from the particular batches that we have purchased using differential scanning calorimetry (DSC) on a TA instrument Q2000 DSC device. The chemical properties of both polyesters are collected in Table I. The PDLLA and PDLGA had a T_g of 50 °C and 47 °C, respectively. These T_g values are above the physiological temperature of 37 °C [21] and hence these materials are adequate for use inside the human body. We also determined the weight averaged molecular weight (Mw) by size exclusion chromatography (SEC) on a Waters GPC Alliance 2695 and obtained values of 367 000 g/mol (with a dispersity of 1.83) and 179 000 g/mol (with dispersity of 1.85) for PDLLA and PDLGA, respectively. The onset degradation temperatures were 365 °C and 340 °C, as determined with a thermogravimetric analysis (TGA) using a TA Instruments Q50 device.

TABLE I
Summary of the Chemical Properties of the Bulk Polyesters

CHEMICAL PROPERTIES	PDLLA	PDLGA
Inherent viscosity [dl/g]	2.0	1.03
Glass transition temperature (T_g) [°C]	50	47
Molecular weight (Mw) [g/mol]	367 000	179 000
Dispersity (Đ) [a.u.]	1.83	1.85
Onset degradation temperature [°C]	365	340

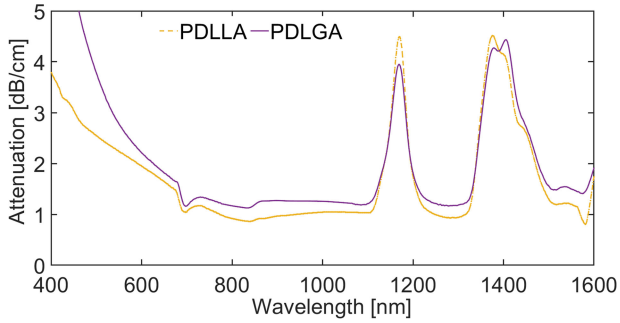

Fig. 1. Attenuation expressed in dB/cm of flat PDLLA and PDLGA sheets fabricated using compression molding.

Prior to preform fabrication, we checked the optical absorption of PDLLA and PDLGA sheets fabricated from the starting granulates using a Jenoptik HEX04 compression molding machine. We measured the direct transmission and specular reflectance spectra with a double beam Jasco V670-EX Spectrophotometer in order to assess the attenuation of the polyesters. Fig. 1 shows attenuation spectra for PDLLA and PDLGA sheets in the VIS-NIR wavelength region. The attenuation values of PDLGA are not far off those of PDLLA: 1.94 dB/cm and 1.78 dB/cm at 633 nm, and 1.17 dB/cm and 0.94 dB/cm at 800 nm. These results indicate that the as-processed PDLLA and PDLGA both feature comparable optical loss in the VIS-NIR wavelength region, which is important in view of forming a core-cladding structure.

The second very important parameter is the refractive index. Note that we have already reported on the refractive index of PDLLA in [20]. We carried out refractive index measurements on PDLGA bulk sample in the VIS spectral range using an Anton Paar Abbemat MW Refractometer at 5 wavelengths in the range of 436 to 656 nm. The measured refractive index data was fitted

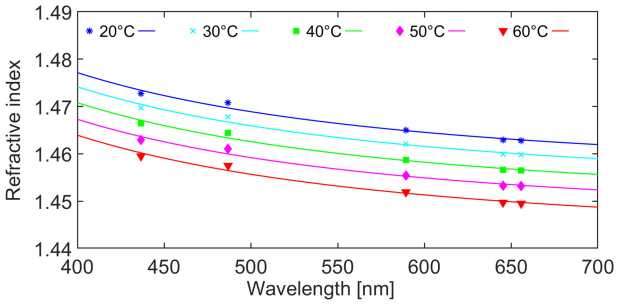

Fig. 2. PDLGA refractive index measured at different temperatures (dots) and Sellmeier equation fits (solid lines).

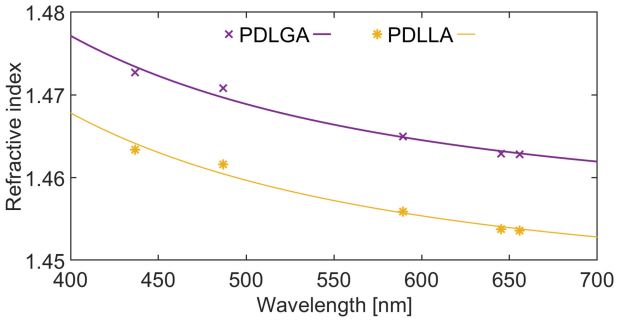

Fig. 3. Comparison of PDLLA (∗) and PDLGA (x) refractive indices measured at 20 °C and Sellmeier equation fits (solid lines). Sellmeier coefficients for PDLLA: $B_1 = 1.0907$, $C_1 = 0.0940$ and for PDLGA: $B_1 = 1.1168$, $C_1 = 0.0939$.

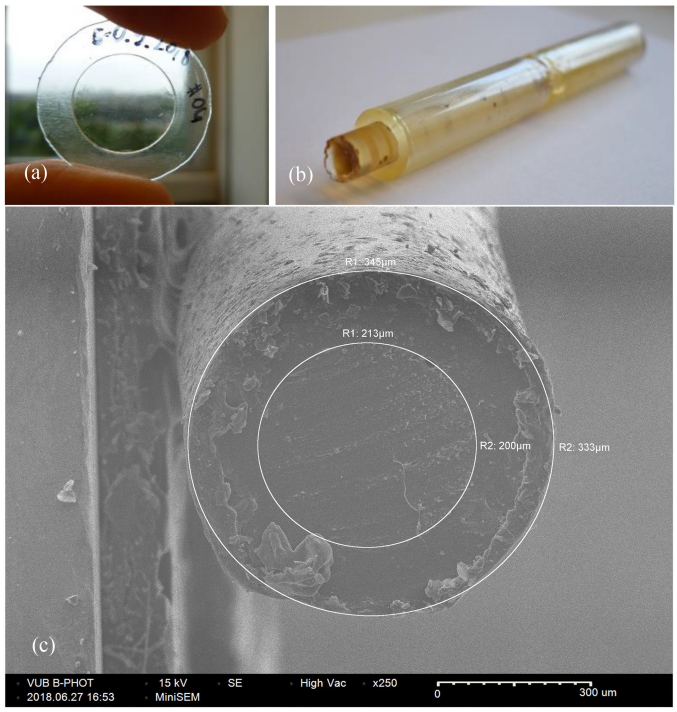

Fig. 4. (a) Photograph of the compression molded PDLGA sheet, (b) Photograph of the preform (P2) consisting of a PDLGA rod inserted into a PDLLA tube. Yellowish discoloration was caused by thermal oxidation. (c) SEM image of the eventual step-index bioPOF, with a core-cladding ratio of about 4:7, where the core radius is around 213–200 μm and the cladding radius is 345–333 μm.

to the Sellmeier dispersion formula [28] given by equation (1):

$$n^2(\lambda) = 1 + \frac{B_1\lambda^2}{\lambda^2 - C_1^2} \tag{1}$$

in which n is the refractive index, λ is the wavelength and B_1 and C_1 are fitting parameters.

Fig. 2 reveals that the refractive index follows a regular dispersion profile for the temperature in the range 20–60 °C. Fig. 3 shows the measurement of the dispersion curve of PDLLA and PDLGA carried out at 20 °C. PDLGA has a larger refractive index and therefore it can serve as core material, whilst PDLLA appears adequate as cladding material. Both polyesters fit within the group of glassy polymers, that are hard and brittle (i.e., PMMA, PC, PS) and that have their dn/dT values in the range of -1–-2×10^{-4} °C^{-1} [29]. For all the wavelengths and in the temperature range below Tg, the thermo-optic coefficient of both polyesters is negative. For PDLGA it is -3×10^{-4} °C^{-1}, whilst for PDLLA it is -1×10^{-4} °C^{-1}. Knowing the thermo-optic coefficients, we also estimated the thermal volumetric expansion coefficients using the Lorentz-Lorenz relation. In [20] we have already reported that the thermal expansion of PDLLA is in the range of 1.92–2.00 $\times 10^{-4}$ °C^{-1}. The thermal expansion coefficient of PDLGA is slightly higher with values in the range 5.7–6.0 $\times 10^{-4}$ °C^{-1}. Both coefficients have the same order of magnitude and are sufficiently close to mitigate against excessive deformation during the drawing process.

III. BioPOF Fabrication

To fabricate the preform of our step-index bioPOF, we used a conventional rod-in-tube technique [30]. We first manufactured dedicated Teflon molds for the PDLGA rod and PDLLA tube that will be turned into the bioPOF's core and cladding, respectively. The tube had a length of 20 cm, an outer diameter of 1.9 cm and an inner diameter 1.2 cm, whilst the rod was 22 cm long and had a diameter of 1.1 cm. The main challenge during the preform fabrication was to avoid the appearance of vacuum voids trapped within the melt due to the high viscosity of the polymer. We tackled this by keeping the polymer in a molten state in the oven for 36 to 48 h at 170 °C. To minimize thermal oxidation of the polyesters, the mold was flushed with Argon. Fig. 4 (b) shows a photograph of one of the preforms.

We fabricated two types of preforms labeled P1 and P2, respectively. The P1 preforms exhibited some fractures due to mechanical demolding. Therefore, two P1 preforms, labeled P1a and P1b were annealed at 180 °C using a hot air gun in order to melt and reconnect the edges of the cracks, whilst the P2 preform (only one has been fabricated) did not receive any further thermal treatment.

We then successfully fabricated three batches of step-index bioPOF (labeled as F1a, F1b and F2) from the three preforms P1a, P1b and P2, respectively, with a standard heat drawing procedure [31]. The preforms were preheated at 100°C, at a rate varying between 5 to 2.5 °C/min, using a furnace with a diameter of around 3 cm. To avoid oxidation of the polymer

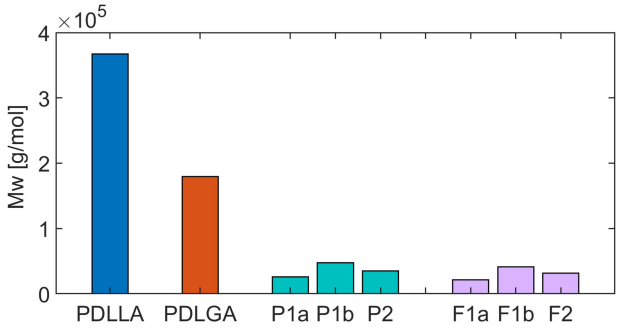

Fig. 5. Molecular weight of PDLLA and PDLGA granulates, of processed preforms (P1a, P1b, and P2) and bioPOFs (F1a, F1b, F2).

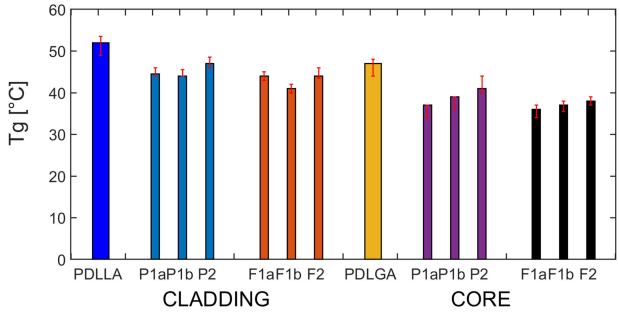

Fig. 6. T_g and indication of the T_g ranges (red range bars) for PDLLA granulate, PDLGA granulate, cladding and core parts from preforms P1a, P1b, P2, and fiber F1a, F1b, F2.

preforms, we flushed it with a constant N_2 flow at 200 l/min. To initiate the drawing, we clamped tongs with a weight of 80 g to the bottom of the preform and we waited for about 15 min for the material to reach drawing temperature. Fibers were drawn at approximately 108 °C. Once the drawing process was initiated and the preform neck-down started, the drawn fiber was taken up by the spinning capstan. We varied the drawing speed between 1 to 1.9 m/min, which allowed controlling the outer fiber diameter from 1000 μm down to 300 μm. Fig. 4 (c) shows a scanning electron microscope (SEM) image of the step-index bioPOF (F2) with a core-to-cladding ratio of about 4:7 (measured dimensions are indicated in the image).

IV. Chemical Characterization of the BioPOF

We carried out SEC and DSC analyses of preforms and fibers. SEC was used to examine the molecular mass of the two polymers. Recall that the starting molecular weights (Mw) were 367 000 g/mol and 179 000 g/mol for PDLLA and PDLGA granulates, respectively. Fig. 5 shows the Mw losses for the 3 preforms P1a, P1b and P2, with values of 93, 87, and 91%, respectively, compared to the Mw of PDLLA granulate. For the same preforms, the Mw reductions were 85, 73 and 81%, compared to the Mw of PDLGA granulate. The prolonged melting time during the perform fabrication caused the substantial molecular mass reduction. The fiber drawing itself had much lesser impact, with a decrease of 19, 14 and 10% for fibers F1a, F1b and F2 compared to the values of preforms P1a, P1b and P2, respectively.

We also measured the T_g of the polymers using DSC. The T_g values decreased after processing into a preform and fiber as shown in Fig. 6, with the largest difference of 10 °C for PDLGA processed into the core of preform P1a and 8 °C for PDLLA processed into the cladding of preform P1b. From the above one can conclude that the preform preparation has the largest influence on the thermo-mechanical properties of the polymers and that the fabrication process is repeatable, since the values are similar for all the preforms and fibers.

V. Optical Characterization of the BioPOF

To measure the spectral attenuation, we applied a standard cutback method [32] and we used a broadband Laser-Driven

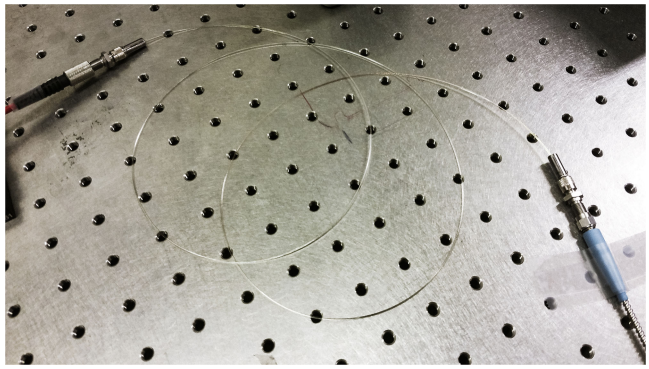

Fig. 7. A section of bioPOF with SMA905 connectors leading to optical fibers.

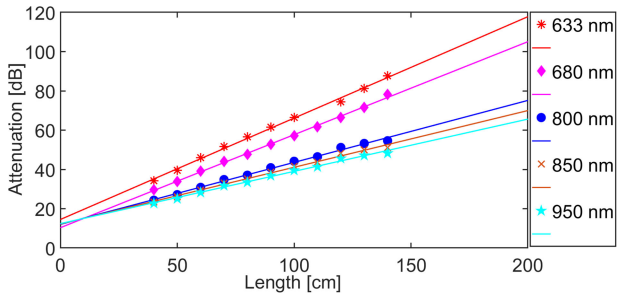

Fig. 8. Cutback measurement result of step-index bioPOF F2 at selected wavelengths. The solid lines are the linear regressions, the slope of which returns the attenuation in dB/cm.

Light Source Model EQ-99X-FC LDLS and an AvaSpec2048 spectrum analyser. Before the measurements, we cleaved the fiber ends using a microtome blade on a hot plate set at around 25–30 °C. The bare fiber-ends were temporarily fixed into a Ø1050 μm bore SS Ferrule for multimode SMA905 connectors [33] and connected with SMA mating sleeves to the source and detection lead optical fibers [34], as pictured in Fig. 7.

The outer diameter averaged over the F2 fiber length was 1000 ± 50 μm, whilst the core had a diameter of 570 ± 30 μm. Fig. 8 shows the results of cutback measurements at five selected wavelengths. The lowest attenuation $\alpha = 0.26$ dB/cm was at 950 nm, which is the lowest loss obtained so far for biodegradable step-index bioPOF [7], [10], [15].

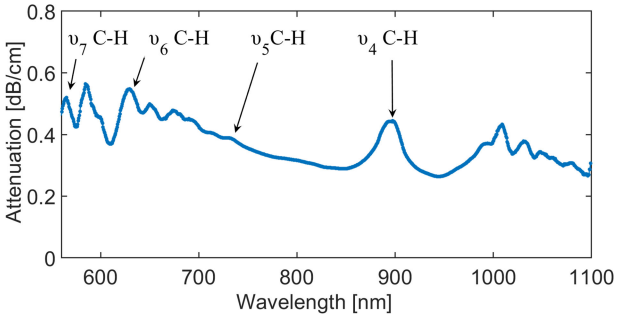

Fig. 9. Spectral attenuation of step-index bioPOF F2 with the lowest loss of 0.26 dB/cm at 950 nm and indication of the absorption peaks.

The measured attenuation of SI bioPOF is significantly lower than the attenuation given for the PDLLA and PDLGA sheets discussed in Section II. This stems from the different processing conditions during fabrication of the sheets (compression molding) and fibers (thermal drawing).

Fig. 9 shows the spectral attenuation of the F2 bioPOF, which reveals the intrinsic absorption maxima in the VIS and NIR region at 560, 630, 730 and 900 nm that stem from C-H stretching vibration overtones [35].

We evaluated the loss at 633 nm of F1 bioPOFs in order to compare it to the loss of F2 using the cutback method. The fiber diameters were 850 μm and 900 μm for F1a and F2, respectively. We coupled light emitted by a HeNe laser into the fibers and we recorded the output power using a Newport 918D-UV-OD3 Silicon Photodetector. Fiber F1a featured a 16% higher attenuation compared to fiber F2.

We also measured the numerical aperture (NA) of our fabricated bioPOFs. The NA is defined by equation (2). However, NA defines the acceptance angle and the latter depends on the surrounding medium, as given in equation (3):

$$NA = \sqrt{n_{core}^2 - n_{clad}^2} \tag{2}$$

$$NA = n_{air} * \sin\theta_A \tag{3}$$

where n_{core} is the refractive index of the core, n_{clad} is the refractive index of the cladding and θ_A the half angle of acceptance [36]. Considering the refractive indices of PDLGA and PDLLA shown in Fig. 2, at 20 °C we have $n_{core} = 1.464$ and $n_{clad} = 1.454$ at 633 nm, resulting in NA = 0.163 and an acceptance angle in air $\theta_A = 9.38°$. Using a HeNe laser and an Edmund Optics Beam Profiler mounted on a translation stage we examined the profile of the beam exiting the bioPOF (as shown in Fig. 10). The F2 bioPOF portion was 70 cm long and had an averaged outer diameter of 1057 $\pm$ 22 μm. The distance z between the fiber facet and the camera screen was adjusted from 0.5 mm to 23 mm to measure the beam spot diameter D given by the 5% intensity level of the beam profile [37] in order to eliminate the modes guided along cladding, whilst the other fiber end was illuminated to achieve overfilled launching conditions. The acceptance angle θ_A is calculated using equation (4). Fig. 11 shows the measured NA.

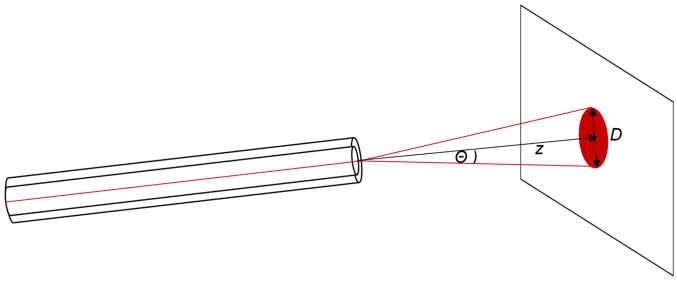

Fig. 10. Illustration of the measurement of NA of the bioPOF.

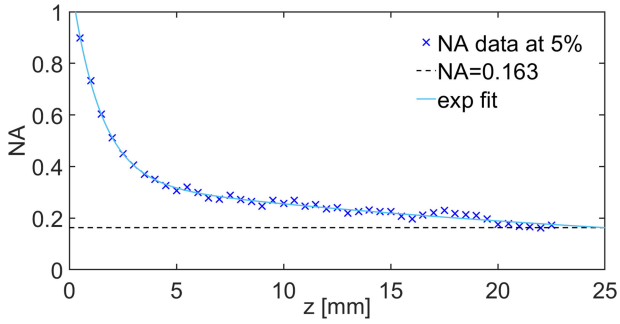

Fig. 11. Relation between the distance z (from the fiber end to the camera) and the NA. The dashed line indicates the value of the previously calculated NA of 0.163.

$$\theta_A = \tan^{-1}\left(\frac{D}{2z}\right) \tag{4}$$

The actual NA is given by the stable value in the far field. With increased distance z above 20 mm, the NA reaches an average value of 0.170 which is close to the calculated value.

During *in vivo* implementation the end facet of the SI bioPOF may be in contact with fluids with a higher refractive index than air. This will impact the value of the half angle of acceptance (θ_A). In case the surrounding medium would have a refractive index close to that of water, i.e., $n_{water} = 1.33$, θ_A would decrease from 9.38° to 7.04°.

Although our SI bioPOF is a multimode fiber with a large core diameter and a relatively low NA with comparison to typical POFs, the guided modes are successfully confined in the core as the evanescent modal field distribution rapidly decays in the cladding. As a result, the guiding efficiency is not affected by any surrounding medium before the degradation of the fiber occurs.

VI. Degradation of BioPOF

A. *In-Vitro Degradation in PBS*

To assess the application potential of our step-index bioPOFs, we investigated their degradation in a simulated biological environment [38]. We did so by immersing fibers with outer diameters of 1000 μm from the three fabrication batches (F1a, F1b and F2), as well as an additional sample of 1000 μm unclad PDLGA fiber in PBS (0.1 M, pH = 7.4), and by incubating

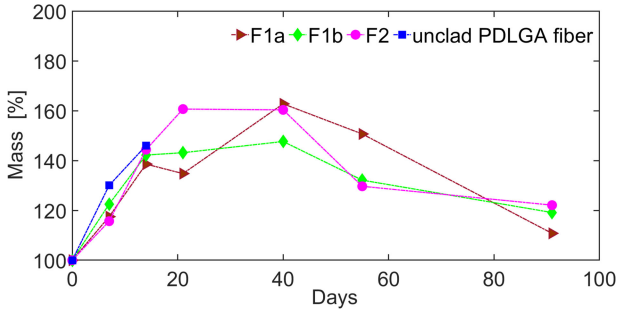

Fig. 12. Mass percentage change of incubated in PBS bioPOFs of 1000 μm diameter F1a, F1b, F2 and unclad PDLGA fiber as a function of immersion time in PBS at pH 7.4, temperature of 37 °C.

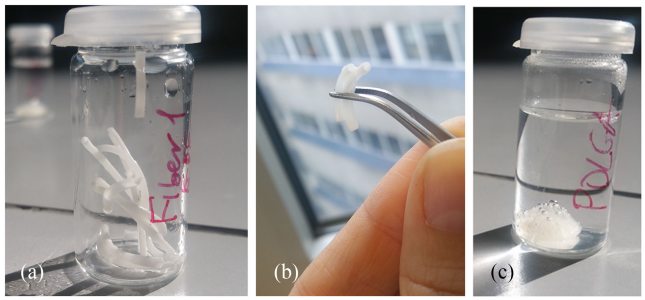

Fig. 13. a) Photograph of F1a SI bioPOF during the degradation study at day 21 b) the F1a fiber revealing absence of the core c) PDLGA fibers on day 21 of the degradation study, essentially reduced to hydrated pulp.

them at 37 °C for a period of about 3 months. Note that we have also attempted to fabricate unclad PDLGA fiber using thermal drawing. The obtained unclad PDLGA fiber was very fragile and difficult to handle. The optical characteristics of such fiber could not be measured, and its mechanical properties would not allow handling in a practical scenario. Therefore, we only deal here with the degradation of this unclad PDLGA fiber for sake of comparison with the results on unclad PDLLA fiber, which we have already addressed in [20] and to reveal possible differences in degradation between PDLLA and PDLGA, considering that our step-index bioPOF involves both materials. We renewed the PBS every week and we analyzed the mass of the fiber samples using a laboratory weighing scale and the Mw using SEC on a Waters GPC Alliance 2695.

During the study, we determined the mass of the fibers as a function of soaking time in PBS after gently removing excess surface water with filter paper and we compared the mass to that prior to incubation. The mass percentage change was determined by the ratio of the incubated samples weight to that of pristine samples.

Fig. 12 reveals a gradual mass increase for all the samples during the first two weeks. Transparent and straight bioPOFs started turning white and swollen after 7 days of immersion. The largest mass growth of 163 and 161% for samples of fibers F1a and F2, and of 148% for a sample of fiber F1b, occurred after 40 days of incubation. Subsequently, we observed a reduction in mass growth caused by the loss of the fiber core. Due to the degradation of the PDLGA, the bioPOFs indeed took the form of a core-shell structure that absorbed less water- see Fig. 13b). Unclad PDLGA fiber sample swelled with a maximum of 146% mass in the first two weeks and up to a degree at which the sample could no longer be handled. The presence of the PDLLA cladding confirms the slowdown of the degradation of PDLGA core. The complete degradation and disintegration of the bioPOFs samples happened after 4 months of incubation.

Unclad PDLLA fibers with a diameter of around 600 μm absorbed PBS at a much slower rate than SI bioPOFs, reaching around 150% mass after 69 days and between 177-152% after 100 days of incubation, as shown in Fig. 14. This is attributed to the more hydrophobic nature of PDLLA, which is due to presence of the methyl group in the repeating unit. Lactic acid is more

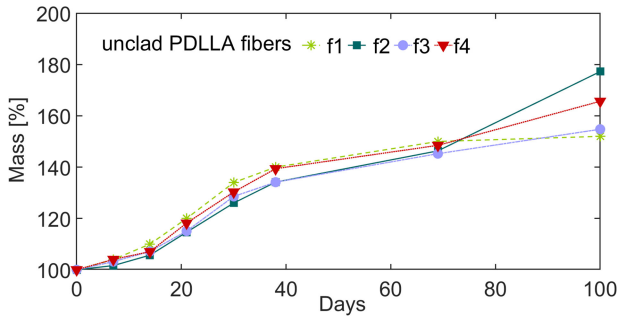

Fig. 14. Mass percentage change of four unclad PDLLA fibers f1, f2, f3 and f4 with a diameter of about 600 μm, as a function of immersion time in PBS at pH 7.4 and 37 °C.

hydrophobic than glycolic acid [39], hence water diffusion into PDLLA samples is delayed compared to PDLGA. Additionally, larger diameter SI bioPOFs (1000 μm) swell and accumulate more PBS, which results in faster degradation than those with smaller diameters, as explained in [20]. This allows concluding that the degradation rate of SI bioPOF can potentially be tuned in view of meeting specific requirements of different application scenarios by controlling the dimensions of core and cladding.

Polymer degradation is essentially a process of polymer molecules breakage. In our bioPOFs, the cleavage of covalent bonds in the polymer backbone initiated in the hydrated regions of the PDLGA and PDLLA leads to a decrease of molecular weight of each polyester. Determining the Mw reduction as a function of incubation time therefore allows quantifying the amount of degradation.

The degradation mechanism of PDLLA and PDLGA fibers is a collective process of bulk diffusion, surface diffusion, bulk erosion and surface erosion. At the initial stage of degradation, water permeates into the polymer chains, causing breakage of ester bonds and generating hydroxyl and carboxyl end groups, whose autocatalytic effect accelerate scission and disentanglement of polymer chains. During the degradation of polymer chains, oligomers and monomers are created. As the rate of molar mass decreases, the low molar mass compounds are eliminated from the polymer matrix, and the catalytic effect of the carboxylic acid groups is lowered [40]. The bulk of fibers degrades faster

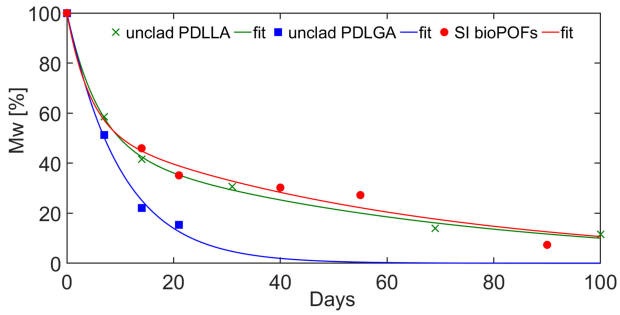

Fig. 15. Mw percentage of SI bioPOF (averaged values of F1a and F1b) and unclad PDLGA (both 1000 μm diameter) and PDLLA fibers (600 μm diameter) immersed in PBS at 37 °C as a function of time. The data sets are fit with solid lines to visualize the exponential decays.

than their surface due to the neutralization of terminal carboxyl groups by PBS.

To describe the degradation with time, we can use a model relying on first order kinetics [41] given by equation (5):

$$Mw(t) = Mw_0 \exp(kt) \tag{5}$$

Mw(t) represents the molecular weight at time *t*, Mw_0 is the initial molecular weight, and -*k* is the degradation rate, with -1/*k* corresponding to the degradation time constant.

Such a kinetic model has been often used to describe the hydrolysis of bioresorbable polyesters. The degradation of PDLLA and SI bioPOF reveals the highest goodness of fit with the sum of two exponential degradation terms ($R^2 = 0.998$ and $R^2 = 0.986$, respectively for SI bioPOF and unclad PDLLA), i.e., a sum of an initially fast and a delayed exponential decay. This is consistent with the data reported in [42]. The molecular weight expressed as a function of time follows equation (6)

$$Mw(t) = Mw_{01} \exp(k_1 t) + Mw_{02} \exp(k_2 t) \tag{6}$$

Mw_{01} is the molecular weight before hydrolysis, Mw_{02} is the molecular weight at the start of the second hydrolysis stage and -k_1 and -k_2 are the kinetic constant rates for each degradation stage.

Fig. 15 shows the degradation of SI bioPOF (averaged values of F1a and F1b) and unclad PDLGA and PDLLA fibers as a function of time in terms of the percentage of remaining molecular weight.

First, the polymer backbone started to break, and the molecular weight substantially decreased due to the penetration of water molecules. Second, the ester groups on the molecular chain were exposed to water and hydrolysis occurred [43]. For PDLLA, the degradation started rapidly at a rate of 0.171 day^{-1} and then decelerated after around 7 weeks down to a rate of 0.0154 day^{-1}, with a final Mw value that decayed down to 12% at the end of the study. Characterizing the step-index bioPOF degradation on the basis of the Mw value is more challenging. It should be mentioned that SEC does not allow distinguishing between components of similar molecular mass. Since the bioPOF consists of two compounds, SEC recorded broad dual-peak molecular weight distributions. The peaks belonging to the individual polymers overlapped, which prevented readily comparing the Mw values of PDLLA and PDLGA following degradation study. The results shown in Fig. 15 indicate that step-index bioPOF degraded in a similar manner to unclad PDLLA fiber. The initial rate of around 0.237 day^{-1} was slightly higher than for unclad PDLLA, most likely due to the PBS penetration into the fiber's center with an initially accelerated degradation of the PDLGA core, followed by a slower 0.0163 day^{-1} rate associated with the degradation of PDLLA. The Mw decayed down to 8.6% after 90 days. As discussed above, the degradation of PDLGA was the most rapid. The Mw of unclad PDLGA fiber decreased down to 15% of the original molecular weight already after 21 days. The Mw reduction of PDLGA occurred with a rate of 0.0985 day^{-1}. The origin of accelerated PDLGA degradation is due to higher content of glycolic acid, which exits the sample approximately twice as fast as lactic acid [44].

Unlike F1a and F1b, fiber F2 of step-index bioPOF did not feature a clear exponential decay. Only after 55 days, the Mw decreased to around 40% of the initial value and dropped down to 11% by the end of the study. This delayed degradation for fiber F2 is most likely due to the seemingly better fabrication quality, to which we will come back in Section VI B.

Note that the degradation is considered complete when oligomeric and low molecular weight fractions are decomposed in the surrounding medium. The final degradation products such as lactic and glycolic acids occur naturally within the metabolic cycle. Hence these will be metabolized and eliminated from the organism without any toxic effect [45].

B. *Immersion Induced Optical Loss*

We evaluated the induced optical losses of bioPOFs with respect to their immersion time in PBS (pH = 7.4) at 37 °C. We coupled light from a broadband Laser-Driven Light Source Model EQ-99X-FC LDLS into the three tested fibers and we measured the power output using an AvaSpec2048 spectrum analyzer. The Immersion Induced Loss (IIL) is defined by equation (7) as:

$$\text{IIL} = \frac{10}{L} * \log_{10} \frac{P(t=0)}{P(t)} \tag{7}$$

where *P* is the measured optical power exiting the fiber, *t* is time and *L* is the length of the immersed fiber portion.

We carried out 3 measurements, labeled IIL_1, IIL_2 and IIL_3 on 3 bioPOF portions with an immersed length of around 23 cm, total length of 100 cm and 90 cm, and outer diameters of 826 $\pm$ 30 μm, 840 $\pm$ 36 μm, and 497 $\pm$ 62 μm, respectively. All samples were kept straight during the experiment.

Fig. 16 displays the IIL values as a function of immersion time at two selected wavelengths for two samples of F1b bioPOF (IIL_1, IIL_2) with larger diameters in the low intrinsic loss windows, i.e., 800 and 950 nm. We observe an immediate gradual loss increase with time for IIL_2 and a 10 minutes delayed loss increase for IIL_1. The smaller diameter fiber (F2) IIL_3 appeared steadier and exhibited no presence of any additional loss at 650 nm during the initial 40 min of soaking, as shown in Fig. 17. There is a very similar behavior of ILL_3 for F2 at NIR wavelengths- see Fig. 18. During the first 14 min, the IIL

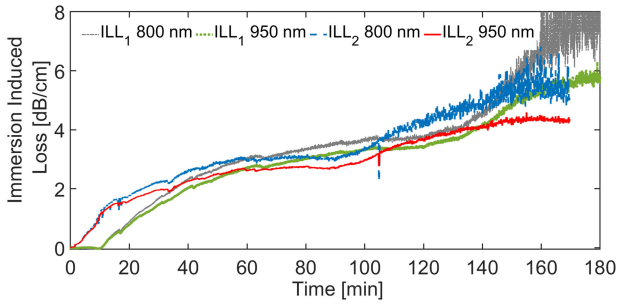

Fig. 16. Immersion induced loss (IIL) at 800 nm and 950 nm of bioPOFs soaked in PBS at 37 °C as a function of immersion time for two F1b fiber samples: with outer diameters 826 ± 30 μm (IIL_1) and 840 ± 36 μm (IIL_2).

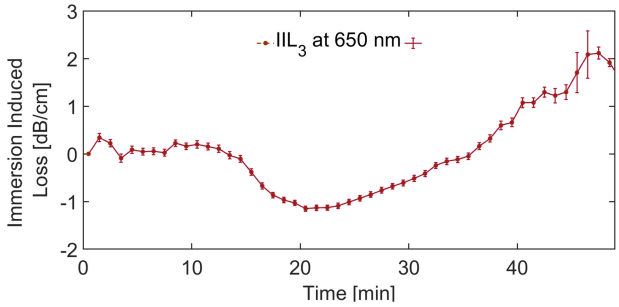

Fig. 17. Immersion induced loss (IIL) at 650 nm of bioPOF soaked in PBS at 37 °C as a function of immersion time during the first 50 min of soaking for a F2 fiber sample with a diameter 497 ± 62 μm (IIL_3).

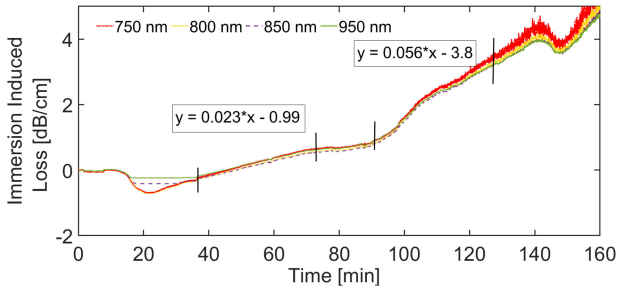

Fig. 18. Immersion induced loss (IIL) of bioPOF soaked in PBS at 37 °C as a function of immersion time for a F2 fiber sample with a diameter 497 ± 62 μm (IIL_3) at chosen NIR wavelengths.

kept stable at approximately 0 dB/cm. Subsequently, we observe an increase of the transmitted power in the fiber for around 26 minutes, once PBS penetrated inside the bioPOF. The initial decrease of the propagation loss is presumably due to either the increase of the NA when the surrounding aqueous medium with lower refractive index infiltrates the cladding or due to reduced scattering at the watered core-cladding interface. The immersion induced loss in the NIR region started growing linearly with a rate of 0.023 dB/cm per minute during the next 40 minutes of soaking, most likely due to the penetration of PBS into the core and the initiation of the degradation process of PDLGA. Once the degradation of the core was initiated, the IIL accelerated to a higher rate of 0.056 dB/cm per minute in the time interval from 100 to 140 minutes.

Both the *in vitro* degradation and the immersion induced loss of bioPOF depend on the fiber dimensions but also on the fiber fabrication quality. F1a and F1b revealed local delamination between core and cladding along the fiber length, which may have affected the faster water penetration and accelerated the increase of immersion induced loss. F2 appeared free of any defect and hence they also exhibited delayed Mw degradation. Additionally, smaller diameter F2 bioPOFs (497 ± 62 μm, see IIL_3) did not feature any additional loss at 650 nm during the initial 40 min of immersion. This agrees well with the immersion-induced loss at 633 nm that we have already conducted for unclad PDLLA fibers with average diameters of 588 ± 41 μm and 523 ± 41 μm. Those fibers did not show immersion-induced loss during the first hour in PBS either [20]. As discussed earlier, larger diameter step-index bioPOFs degrade faster than smaller fibers. The higher IIL growth rate for thicker F1b bioPOFs is caused by easier access of PBS to the sample's center and confirms that the degradation of poly-(lactic acids) based material is initiated within the fiber's bulk. Since PDLGA degrades faster than PDLLA, the IIL of SI bioPOF with a PDLGA core increases at a higher rate than unclad PDLLA fiber.

VII. Conclusions

We demonstrated the fabrication of truly biodegradable step-index polymer optical fiber using commercially available polyesters known as PDLGA and PDLLA. PDLGA is used as core material whilst PDLLA forms the cladding of the bioPOF. Both polyesters are suited for fiber drawing using a conventional optical fiber draw tower. We obtained bioPOFs with a NA of 0.107 and record low attenuation of 0.26 dB/cm at 950 nm.

We evidenced the *in vitro* degradation of our bioPOFs with an average outer diameter of 1000 μm: the averaged molecular weights decreased down to 8.6% of the original values after 3 months of incubation in PBS. The bioPOFs take up PBS with mass increases up to 160%, which indicates the excellent permeability of the fibers to water.

Predicting the *in vivo* degradation rate of bioPOFs based on our *in vitro* results is challenging though. We can nevertheless refer to [46] which reported on the lower solubility of bioresorbable optical fibers in animal body. The slower degradation was attributed to the encapsulation of the fiber in tissue that limits contact with renewed physiological fluid. Additionally, the magnitude of tissue response to a resorbable material significantly depends upon the implantation site [47]. The evolution of *in vivo* optical loss of our bioPOFs should therefore be examined.

The processing of the poly(lactic-acid) materials into preforms was successful, yet melting of the starting granulates into preforms and maintaining the molten state over a prolonged time to avoid the occurrence of vacuum voids led to a substantial molecular mass reduction. We anticipate that better control over molecular mass decrease is possible using a different preform manufacturing method, for example injection molding. Additional care also has to be taken to avoid local delamination between core and cladding. The fabrication quality and post-processing of the preforms using heat treatment, influences the optical performance and degradation rate of the bioPOFs

drawn from such preforms. These features can nevertheless be exploited in view of tuning the degradation rate of bioPOF to particular application scenarios. Another parameter that can contribute to controlling the degradation rate is the comonomer ratio of D,L-lactide to glycolide of PDLGA, that forms the step-index bioPOF core. The latter would also enable tuning the refractive index differences between core and cladding. Finally, adapting the core and cladding diameters would allow for additional control over the degradation rate.

Based on our results, we can project the use of smaller diameter step-index bioPOF ($<$500 μm) in photodynamic therapy applications, owing to their stability in terms of optical loss during the first 30 minutes [48], [49] of immersion and their good transmission properties at 650 nm, which corresponds to the operation wavelength of photosensitizers that are typically used for such purposes (i.e., methylene blue) [50].

Moreover, our results open interesting perspectives for exploiting these biodegradable polymer optical fibers for deep tissue penetration. Micro-structured or core-shell optical fibers could be suitable candidates for controlled delivery of therapeutics. Owing to the good water permeability, they will demonstrate the absorption of surrounding body fluids *in vivo* and may have an effect on the transfer of metabolites throughout the fiber device [51]. Furthermore, light-triggered rapid drug release, that can be achieved in around 20–30 minutes using near infrared light transmitted through our bioPOF could be an interesting approach in a cancer therapy [52].

REFERENCES

[1] T. Meyer, M. Schmitt, O. Guntinas-Lichius, and J. Popp, "Toward an all-optical biopsy," *Opt. Photon. News*, vol. 30, no. 4, pp. 26–33, 2019.

[2] L. Ylikontiola, K. Sundqvuist, G. K. B. Sàndor, P. Törmälä, and N. Ashammakhi, "Self-reinforced bioresorbable poly-L/DL-Lactide [SR-P(L/DL)LA] 70/30 miniplates and miniscrews are reliable for fixation of anterior mandibular fractures: A pilot study," *Oral Surg. Oral Med. Oral Pathol. Oral Radiol. Endodontol.*, vol. 97, no. 3, pp. 312–317, 2004.

[3] D. R. Sparta, A. M. Stamatakis, J. L. Phillips, N. Hovelsø, R. Van Zessen, and G. D. Stuber, "Construction of implantable optical fibers for long-term optogenetic manipulation of neural circuits," *Nature Protocols*, vol. 7, no. 1, pp. 12–23, 2011.

[4] E. Ceci-Ginistrelli *et al.*, "Novel biocompatible and resorbable UV-transparent phosphate glass based optical fiber," *Opt. Mater. Exp.*, vol. 6, no. 6, pp. 2040–2051, 2016.

[5] D. Pugliese *et al.*, "Bioresorbable optical fiber Bragg gratings," *Opt. Lett.*, vol. 43, no. 4, pp. 671–674, 2018.

[6] A. Dupuis *et al.*, "Prospective for biodegradable microstructured optical fibers," *Opt. Lett.*, vol. 32, no. 2, pp. 109–111, 2007.

[7] M. B. Applegate, G. Perotto, D. L. Kaplan, and F. G. Omenetto, "Biocompatible silk step-index optical waveguides," *Biomed. Opt. Exp.*, vol. 6, no. 11, pp. 4221–4227, 2015.

[8] K. H. Tow, D. M. Chow, F. Vollrath, I. Dicaire, T. Gheysens, and L. Thevenaz, "Exploring the use of native spider silk as an optical fiber for chemical sensing," *J. Lightw. Technol.*, vol. 36, no. 4, pp. 1138–1144, Feb. 2018.

[9] M. Choi, J. W. Choi, S. Kim, S. Nizamoglu, S. K. Hahn, and S. H. Yun, "Light-guiding hydrogels for cell-based sensing and optogenetic synthesis in vivo," *Nature Photon.*, vol. 7, no. 12, pp. 987–994, 2013.

[10] M. Choi, M. Humar, S. Kim, and S. H. Yun, "Step-index optical fiber made of biocompatible hydrogels," *Adv. Mater.*, vol. 27, pp. 4081–4086, 2015.

[11] J. Guo *et al.*, "Highly stretchable, strain sensing hydrogel optical fibers," *Adv. Mater.*, vol. 28, no. 46, pp. 10244–10249, 2016.

[12] A. K. Yetisen *et al.*, "Glucose-sensitive hydrogel optical fibers functionalized with phenylboronic acid," *Adv. Mater.*, vol. 29, no. 15, 2017, Art. no. 1606380.

[13] S. Nizamoglu *et al.*, "Bioabsorbable polymer optical waveguides for deep-tissue photomedicine," *Nature Commun.*, vol. 7, no. 10374, pp. 1–7, 2016.

[14] R. Fu, W. Luo, R. Nazempour, D. Tan, H. Ding, and K. Zhang, "Implantable and biodegradable poly (l -lactic acid) fibers for optical neural interfaces," *Adv. Opt. Mater.*, vol. 6, no. 3, pp. 1–8, 2017.

[15] D. Shan *et al.*, "Flexible biodegradable citrate-based polymeric step-index optical fiber," *Biomaterials*, vol. 143, pp. 142–148, 2017.

[16] S. Park *et al.*, "One-step optogenetics with multifunctional flexible polymer fibers," *Nature Neurosci.*, vol. 20, no. 4, pp. 612–619, 2017.

[17] R. Nazempour, Q. Zhang, R. Fu, and X. Sheng, "Biocompatible and implantable optical fibers and waveguides for biomedicine," *Mater. (Basel)*, vol. 11, no. 1283, pp. 1–21, 2018.

[18] M. Humar, S. J. J. Kwok, M. Choi, A. K. Yetisen, S. Cho, and S. H. Yun, "Toward biomaterial-based implantable photonic devices," *Nanophotonics*, vol. 6, no. 2, pp. 414–434, 2017.

[19] D. Shan *et al.*, "Polymeric biomaterials for biophotonic applications," *Bioactive Mater.*, vol. 3, no. 4, pp. 434–445, 2018.

[20] A. Gierej *et al.*, "Poly(D,L-lactic acid) (PDLLA) biodegradable and biocompatible polymer optical fiber," *J. Lightw. Technol.*, vol. 37, no. 9, pp. 1916–1923, May 2019.

[21] H. K. Makadia and S. J. Siegel, "Poly lactic-co-glycolic acid (PLGA) as biodegradable controlled drug delivery carrier," *Polym. (Basel)*, vol. 3, pp. 1377–1397, 2011.

[22] F. Quaglia, "Bioinspired tissue engineering: The great promise of protein delivery technologies," *Int. J. Pharmaceutics*, vol. 364, no. 2, pp. 281–297, 2008.

[23] F. T. INC, "ZILRETTA extended-release dosage form consisting of microspheres of poly(lactic-co-glycolic acid) (PLGA)," 2017. [Online]. Available: https://www.accessdata.fda.gov/drugsatfda_docs/label/2017/208845s000lbl.pdf. Accessed: Feb. 14, 2019.

[24] W. Bai *et al.*, "Bioresorbable photonic devices for the spectroscopic characterization of physiological status and neural activity," *Nature Biomed. Eng.*, vol. 3, no. 8, pp. 644–654, 2019.

[25] U.S. Food and Drug Administration, "Drug Master Files (DMFs)-FDA Guidance," May 2015. [Online]. Available: https://www.fda.gov/media/86792/download. Accessed: Dec. 25, 2019.

[26] Corbion, "Polymers for medical devices," 2019. [Online]. Available: https://www.corbion.com/static/downloads/datasheets/30d/purasorb%20pdl%2020.pdf, Accessed: Dec. 25, 2019.

[27] Polymers for drug delivery, "Purasorb PDLG 5010." 2019. [Online]. Available: https://www.corbion.com/static/downloads/datasheets/36d/purasorb%20pdlg%205010.pdf. Accessed: Dec. 25, 2019.

[28] M. G. Kuzyk, *Polymer Fiber Optics Materials, Physics, and Applications*. Boca Raton, FL, USA: CRC, 2007.

[29] P. A. Soave, R. A. F. Dau, M. R. Becker, M. B. Pereira, and F. Horowitz, "Refractive index control in bicomponent polymer films for integrated thermo-optical applications," *Opt. Eng.*, vol. 48, no. 12, 2009, Art. no. 124603.

[30] Q. Chen, H. Wang, Q. Wang, Q. Chen, and Y. Hao, "Modified rod-in-tube for high-NA tellurite glass fiber fabrication: Materials and technologies," *Appl. Opt.*, vol. 54, no. 4, pp. 946–952, 2015.

[31] M. Beckers, T. Schlüter, T. Vad, T. Gries, and C.-A. A. Bunge, "An overview on fabrication methods for polymer optical fibers," *Polym. Int.*, vol. 64, no. 1, pp. 25–36, 2015.

[32] *Optical Fibres - Part 1-40: Measurement Methods and Test Procedures - Attenuation*, IEC 60793-1-40:2001, 2001.

[33] Thorlabs Inc., "B11050A - SMA905 Multimode Connector, Ø1050 μm Bore, SS Ferrule, for BFT1," 2018. [Online]. Available: https://www.thorlabs.com/thorproduct.cfm?partnumber=B11050A

[34] Avantes, "Fiber-optic Cables - Avantes, FC-UVIR600-2," 2018. [Online]. Available: https://www.avantes.com/images/12_Fiber-optic_Cables.pdf. Accessed: Dec. 25, 2019.

[35] A. Rousseau and B. Boutevin, "Synthesis of low absportion halogenated polymers for POF," in *Proc. Plastic Opt. Fibres Appl. Conf.*, Paris, France, 1992, pp. 33–37.

[36] T. G. Brown, "Optical fibers and fiber-optic communications," in *Fiber Optics Handbook: Fiber, Devices and Systems for Optical Communications*. New York, NY, USA: McGraw-Hill, 2002, pp. 1–50.

[37] Optical Fibres - Part 1-43: Measurement Methods and Test Procedures - Numerical Aperture Measurement, IEC 60793-1-43:2015, 2015.

[38] K. Shi *et al.*, "Synthesis, characterization, and application of reversible PDLLA-PEG-PDLLA copolymer thermogels in vitro and in vivo," *Sci. Rep.*, vol. 6, no. 19077, pp. 1–15, 2016.

[39] Z. Ma, N. Zhao, and C. Xiong, "Degradation and miscibility of poly(DL-lactic acid)/poly(glycolic acid) composite films: Effect of poly(DL-lactic-co-glycolic acid)," *Bull. Mater. Sci.*, vol. 35, no. 4, pp. 575–578, 2012.

[40] M. Vert, "Aliphatic polyesters: Great degradable polymers that cannot do everything," *Biomacromolecules*, vol. 6, pp. 538–546, 2005.

[41] C. G. Pitt and G. Zhong-wei, "Modification of the rates of chain cleavage of poly(ε-caprolactone) and related polyesters in the solid state," *J. Control Release*, vol. 4, pp. 283–292, 1987.

[42] E. J. Rodriguez, B. Marcos, and M. A. Huneault, "Hydrolysis of polylactide in aqueous media," *J. Appl. Polym. Sci.*, vol. 133, no. 44, pp. 1–11, 2016.

[43] F. Lin, X. Wang, Y. Wang, Y. Yang, and Y. Li, "Preparation and biocompatibility of electrospinning PDLLA/β-TCP/collagen for peripheral nerve regeneration," *RSC Adv.*, vol. 7, no. 66, pp. 41593–41602, 2017.

[44] A. Göpferich, "Mechanisms of polymer degradation and erosion," *Biomaterials*, vol. 17, pp. 103–114, 1996.

[45] A. L. Sisson, M. Schroeter, and A. Lendlein, "Polyesters," in *Handbook of Biodegradable Polymers: Synthesis, Characterization and Applications*. Hoboken, NJ, USA: Wiley, 2011, pp. 1–21.

[46] O. Podrazký *et al.*, "In-vivo testing of a bioresorbable phosphate-based optical fiber," *J. Biophoton.*, vol. 12, no. 7, 2019, Art. no. e201800397.

[47] L. Ferreira *et al.*, "Biocompatibility of chemoenzymatically derived dextran-acrylate hydrogels," *J. Biomed. Mater. Res.—Part A*, vol. 68, pp. 584–596, 2004.

[48] W. M. Star, "Light delivery and light dosimetry for photodynamic therapy," *Lasers Med. Sci.*, vol. 5, no. 2, pp. 107–113, 1990.

[49] J. Shan *et al.*, "Pegylated composite nanoparticles containing upconverting phosphors and meso-tetraphenyl porphine (TPP) for photodynamic therapy," *Adv. Functional Mater.*, vol. 21, no. 13, pp. 2488–2495, 2011.

[50] J. P. Tardavio *et al.*, "Methylene blue in photodynamic therapy : From basic mechanisms to clinical applications," *Photodiagnosis Photodyn. Therapy*, vol. 2, pp. 175–191, 2005.

[51] K. Wanawananon, S. E. Moulton, G. G. Wallace, and S. Liawruangrath, "Fabrication of novel core–shell PLGA and alginate fiber for dual-drug delivery system," *Polym. Adv. Technol.*, vol. 27, no. 8, pp. 1014–1019, 2016.

[52] D. Luo *et al.*, "Rapid light-triggered drug release in liposomes containing small amounts of unsaturated and porphyrin–phospholipids," *Small*, vol. 12, no. 22, pp. 3039–3047, 2016.